

# Stirring N-body systems II: Necessary conditions for the dark matter attractor

Jeremy A. Barber<sup>1\*</sup>, Hongsheng Zhao<sup>1</sup> and Steen H. Hansen<sup>2</sup>

<sup>1</sup>*SUPA, University of St Andrews, North Haugh, St Andrews, Fife, KY16 9SS, UK*

<sup>2</sup>*Dark Cosmology Centre, Niels Bohr Institute, University of Copenhagen, Juliane Maries Vej 30, 2100 Copenhagen, Denmark*

Accepted —. Received —

## ABSTRACT

We study the evolution of the phase-space of collisionless N-body systems under repeated stirrings or perturbations, which has been shown to lead to a convergence towards a limited group of end states. This so-called attractor was previously shown to be independent of the initial system and environmental conditions. However the fundamental reason for its appearance is still unclear. It has been suggested that the origin of the attractor may be either radial infall (RI), the radial orbit instability (ROI), or energy exchange which, for instance, happens during violent relaxation. Here we examine the effects of a set of controlled perturbations, referred to as ‘kicks’, which act in addition to the standard collisionless dynamics by allowing pre-specified instantaneous perturbations in phase-space. We first demonstrate that the attractor persists in the absence of RI and ROI by forcing the system to expand. We then consider radial velocity kicks in a rigid potential and isotropic velocity kicks, since there are no energy exchanges in these two recipes of kicks. We find that these kicks do not lead to the attractor, indicating that the energy exchange in a dynamic potential is indeed the physical mechanism responsible for the attractor.

**Key words:** galaxies: haloes, galaxies: kinematics and dynamics, methods: N-body simulations, methods: numerical

## 1 INTRODUCTION

It is known that N-body simulations tend to yield a narrow range of density profiles for stellar bulges or dark halos (Dubinski & Carlberg 1991, and references therein). These are often parameterised using sub-families of profiles of Zhao (1996) such as the Hernquist profile (Hernquist 1990) for stellar spheroids or the NFW profile (Navarro et al. 1996) for halos. These density profiles and corresponding velocity anisotropy profiles are a result of the energy and angular momentum distribution of particles in the simulation (Hernquist & Spergel 1992), especially how particles exchange their energy and angular momentum, as well as the dynamical friction/tidal disruption of subclumps and the absence/existence of an expanding cosmic background (Syer & White 1998; Taylor & Navarro 2001).

Any N-body code must have its physical laws for such things programmed into it *a priori*, an act which implies that those laws and their implications are comparatively well understood. This paper is part of an ongoing investigation into an *unexpected* result, namely the identification of an attrac-

tor in the phase space of N-body systems, as discussed in Hansen et al. (2010). The attractor is a single-valued relationship between parameters of the Jeans equation; parameters which could have been entirely independent.

The formulation of the Jeans equation that we make use of is:

$$v_c^2 = -\sigma_r^2(\gamma + \kappa + 2\beta) \quad (1)$$

where  $v_c$  is the circular speed,  $\sigma_r^2$  is the radial velocity dispersion,  $\gamma$  and  $\kappa$  are the gradients of  $\log(\rho)$  and  $\log(\sigma_r^2)$  respectively with respect to  $\log(r)$ , and finally  $\beta$  is the velocity anisotropy.

The ‘attractor’ relationship appears if an arbitrary system was repeatedly randomly perturbed away from equilibrium and then allowed to settle again. The perturbations consist of an alternating cycle of perturbations, referred to as ‘kicks’, with a subsequent period of relaxation to a new equilibrium state, referred to as the ‘flow’.

The kicks are a set of controlled, artificial perturbations which act in addition to the standard collisionless dynamics by allowing pre-specified perturbations in phase-space. These perturbations were often constructed to be instantaneous and in most previous studies these kicks allowed en-

\* E-mail: jab22@st-andrews.ac.uk (JAB); hz4@st-andrews.ac.uk (HZ); hansen@dark-cosmology.dk (SH)

ergy exchange amongst a set of particles, even though these particles have negligible two-body energy exchange.

A system perturbed with such repeated kick-flows demonstrates a strong tendency to equilibrate along solutions, regardless of the initial characteristics of the perturbed system (Barber et al. 2012; Sparre & Hansen 2012b), as follows:

$$\beta = \frac{-0.15\gamma - 0.85\kappa}{(1 + (-0.15\gamma - 0.85\kappa)^3)^{\frac{1}{3}}}. \quad (2)$$

This is not the first time that relations and constraints have been discovered in components of the Jeans equation, nor is it the first time specific relations between  $\beta$  and  $\gamma$  have been identified (Hansen 2004; An & Evans 2006; Ciotti & Morganti 2010).

Our previous paper primarily focused on the bulk properties of the initial system and the statistics of the perturbation schemes being used. In this paper we focus on the fundamental requirements of the emergence of this attractor phenomenon.

This is particularly relevant for observations as, depending on the physics responsible for the attractor, it may be either be irrelevant for cosmological structure or it may be of fundamental importance to all equilibrated structures. As we will explain, the attractor may appear due to physics which happens during each merger throughout the history of structure formation. We will demonstrate that this is the case, rendering the attractor potentially very important for the equilibrated part of all cosmological structures, in agreement with the results of large cosmological simulations (Ludlow et al. 2010).

This paper focuses on the origin of the attractor in spherically averaged quantities in an effort to find out what the driving factors for the convergence are. For comparison two recent papers, Sparre & Hansen (2012a,b), discuss how the attractor does appear in the spherically averaged characteristics of many halos but becomes more complicated when the merger history of the object is considered. Those works, using radially-aligned, conical bins rather than spherical averages, find deviations from the attractor along preferred axes defined by the vectors along which past mergers had taken place. However, spherically averaged properties still follow the attractor in most cases.

As this work uses the same analysis pipeline as our previous paper, Barber et al. (2012) (hereafter B12), a detailed description of the method can be found there. In summary we use NMODY, a particle-mesh code developed for use with Modified Newtonian Dynamics (Ciotti et al. 2006), although it is used only in its purely Newtonian mode here. The systems used throughout this paper are Plummer spheres of scale radius 0.05 kpc, containing  $5 \times 10^8 M_{\odot}$  in 750,000 particles. Plummer spheres were chosen as they are formally unrelated to the NFW profile and are easy to create with varying anisotropies using the methods of Gerhard (1991), based on using a particular distribution function into two independent functions that represent the distribution of energy and angular momentum respectively.

The paper is structured as follows: §2 will be on the effect of collision and resolution, §3 will be on radial infall and the radial orbit instability, §4 gives two recipes to avoid the attractor and §5 concludes.

## 2 IMPACT OF NUMERICAL RESOLUTION EFFECTS

We begin by examining the possibility of a connection between our results and the numerical resolution of our simulations; the suggestion being that our conclusions were heavily influenced by numerical artifacts rather than by the physics of the system. Of specific concern was whether the behaviour we were describing could be caused by collisional relaxation and would thus be governed by the softening length of the simulation.

NMODY uses a self-consistent field (SCF) method similar to that described in Hernquist & Ostriker (1992) *i.e.* it describes the potential and density by expanding them into a series of terms in some basis functions. Ciotti et al. (2006) is mainly concerned with demonstrating accurate recovery of MONDian potential-density pairs via this method and thus does not spend time looking at the impact of resolution explicitly. However, the two methods are sufficiently similar that informative results can still be found by examining the impact of numerical resolution in the Hernquist & Ostriker (1992) method.

This work showed that for a variety of initial density models the relative importance of each subsequent term in the basis series decreases exponentially for Plummer models such as ours, providing better than 1% accuracy, in terms of orbit conservation, when using around 5 terms in the series. It is noted that cored models, such as a Plummer sphere, can be particularly well described by this kind of expansion method if the basis functions are chosen appropriately.

Having demonstrated the accuracy of the method, Hernquist & Ostriker (1992) examines the emergence of collisional relaxation in the such a simulation. As there is no explicit softening length used in the method they note that an SCF code should not suffer from limitations on spatial resolution and can, in principle, resolve much steeper density gradients than other methods. Overall, from the conclusion of this paper, we would expect that a code such as NMODY would be efficient at suppressing relaxation noise as only a handful of basis terms are required to provide ample spatial resolution for the simulation.

With this in mind, to explicitly examine the impact of smoothing lengths and resolution on our simulations, several supplementary simulations were run that fell into one of two categories; rougher or smoother models, *cf.* figure 1.

Rougher models lowered the resolution of the model in two ways. Firstly, when the code developed the spherical harmonics that described the potential it used twice the number of terms in the series, making the potential more variable on shorter scales and thus magnifying the effect of short distance interactions. This approach was used rather than simply changing the smoothing length because, as previously discussed, NMODY does not support the direct selection of a desired smoothing length due to the self-consistent field scheme.

Secondly, the initial conditions modelled the same systems as in B12, but now using half the number of particles. This preserved the dynamical timescale of the system while also making the particle distribution noisier. Overall, we would expect the combination of these two effects to emphasise any effects from collisions and, if they are driving the attractor, to lead to the attractor faster.

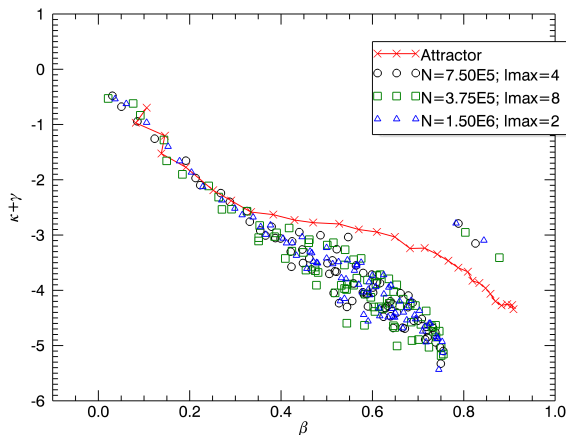


**Figure 1.** Attractor plot demonstrating that there are negligible two-body interactions. It shows the state of three simulations approximately one third (in terms of elapsed time) of the way towards convergence with the attractor (red line). All three use the violent exchange algorithm outlined in B12 with scaling factor 0.5 and  $3T_{dyn}$  flow time per kick. Our benchmark simulation from B12 (black circles) overlaps comfortably with both the rougher (green squares) and smoother (blue triangles) bins of the newer simulations demonstrating a very similar rate of convergence. This shows that the evolution of our systems towards the attractor, which is where they eventually rest, is unaffected by the resolution of the simulations and, consequently, by collisional effects.

Smoother simulations use the same reasoning except they halved the number of terms in the harmonics, effectively smoothing out perturbations on short length scales, and had double the number of particles modelling the system which should smooth the distribution overall. If artificial numerical collisions were governing the attractor, then the de-emphasis of short scale interactions and the smoother particle distribution should suppress the effect.

Overall, these rough/smooth schemes allow us to control the resolution and susceptibility of the system to collisional effects and short-scale interactions while retaining comparable simulations that, as a practical benefit, require comparable amounts of processing time to yield results.

To demonstrate this, we present figure 1 which shows the state of three comparable simulations 10 kick-flow cycles (10 perturbing events spaced evenly throughout a total simulation time of 30 dynamical times). This is approximately one third of the time required for the systems to reach the attractor, given the chosen magnitude of the perturbation according to B12, and demonstrates that the systems are indistinguishable from each other in terms of the parameter space they occupy. Our simulations eventually end up lying in the parameter space of the attractor in a manner indistinguishable from the results from B12. In particular we establish that the behaviour is preserved down to the speed at which the convergence occurs.

The same rougher/smooth dichotomic scheme was applied to a new perturbation method that performs systematic alterations to the system’s velocity anisotropy profile. This new perturbation method will be explained in detail

in §4.1 and it is mentioned here only insofar as to make clear that it also appears unaffected by alterations to the smoothing of the potential.

In summary, the attractor effect is demonstrated to progress the same regardless of the number density of the system or how accurately the simulation models short-scale behaviour and is present in simulations that use different codes (Hansen et al. (2010) used GADGET-2 which has a different architecture to NMODY) to solve for the particles motions. Accordingly, it is not thought that the attractor shares any significant causal link to collisional relaxation or any effect deriving from two-body interactions.

### 3 RULING OUT RADIAL INFALL BY ADDING ENERGY

A characteristic feature of the previous simulations from B12 was a significant amount of radial infall (RI) whereby systems would collapse into more radially anisotropic systems as they were kicked. The fact that all the simulations shared this common mechanism raises the question of whether or not RI is a contributing factor to the attractor.

#### 3.1 Algorithm for avoiding infall

To examine whether or not RI is necessary for the attractor we now use a variation of the scheme from B12 whereby random numbers were used to scale the three cartesian velocity vectors of the system’s particles, however it dispenses with the now redundant routines for assessing energy conservation for reasons that will be explained shortly. The scheme is now as follows:

- Set up a series of radial bins. We chose to create bins defined to contain 5,000 particles.
- For each particle in each bin we examine each of the three orthogonal velocity vectors and multiply each by a random number  $f$  drawn from a uniform distribution centered around 1.5 e.g.  $1.0 < f < 2.0$ . This instantaneous perturbation is referred to as the ‘kick’ and  $f$  can be called the ‘kick scale factor’. That the distribution is *not* centred on unity is what lends *this* scheme its desired asymmetry, as any given velocity component will be at least as big as it was prior to this scaling.
- Derive a dynamical timescale for the system

$$t_{dyn} = \sqrt{\frac{1}{G\rho}} \text{ where } \rho = \frac{0.95 \times M_{tot}}{\frac{4}{3}\pi r_{95\%}^3} \quad (3)$$

where we are using the 95<sup>th</sup> mass percentile as a representative distance for the system. For our initial systems this is equivalent to approximately 3 scale radii and is identical to the previous method.

- The system is then left to evolve in an  $N$ -body simulator for 3 dynamical timescales. This ‘flow’ period allows the system to relax and find a new equilibrium. If we were to apply another kick too soon then the impact of the second kick would be indistinguishable from that of the first.
- Repeat the cycle as needed.

This kick can only be applied a finite number of times before a significant number of particles become unbound from the system. After a large amount of particles become

unbound they will no longer interact with each other and the system ceases to have a meaningful dynamical time. We find that for this particular kick this effect starts to dominate around the fifth kick cycle by which point the outermost 50 bins, *i.e.* 250,000 particles or a third of the entire system, have become entirely unbound from the structure. At this point the simulation is manually halted as the divergent behaviour of the dynamical timescale becomes insurmountable as well as increasingly physically meaningless.

### 3.2 Relation between RI and Radial Orbit Instability

The link between the perturbation used in B12 and RI was in how the system conserved energy. The perturbation in B12 performed the scaling on the components of velocity  $v_{x,y,z}$  but then proceeded to conserve energy in the form of  $v^2$ . This meant that the conservation was asymmetrical compared to the perturbation as  $|(v+\delta v)^2 - v^2| > |(v-\delta v)^2 - v^2|$  unlike the *perturbation* where  $|(v+\delta v) - v| = |(v-\delta v) - v|$  *i.e.* the particles that had their overall velocity increased were contributing more to the kinetic energy of the bin than was being removed by particles which had their velocities decreased by the same amount, leading to an overall increase in energy. The energy conservation code worked on all particles equally, so most particles in a bin ended up losing energy overall to compensate for the small fraction of particles which got large velocity increases and thus significant energy increases. This sudden removal of energy resulted in the compaction of the system and placed many more particles on more radial, infalling orbits.

The main concern was that if RI proved to be necessary for the attractor, and the algorithm was artificially inducing such an infall, then the attractor may just be an artifact of the perturbation scheme. This was compounded by the fact that the radial orbit instability (ROI) displays several convergent behaviours in the parameter spaces of  $\beta$  and  $\gamma$ , as outlined in many papers over the years (Huss et al. 1999; Barnes et al. 2005; Hansen & Moore 2006; Hansen et al. 2006; Macmillan & Henriksen 2006; Bellovary et al. 2008; Lapi & Cavaliere 2011), which bear some noticeable similarities to the attractor.

ROI refers to the unstable nature of orbits in initially spherically symmetric systems which have a large population of their particles on highly radial orbits. Systems set up in this way will depart from spherical equilibrium and will eventually become triaxial systems (Antonov 1973). This behaviour was seen in the majority of the simulations from B12, only noticeably milder than one would expect from a system governed by ROI due to the mild nature of the perturbation. It was therefore suggested that the attractor was being driven by the statistical effects of the kick that caused RI. The increased amount of radial orbits could then lead to ROI which would slowly dominate the system giving rise to the convergent behaviours in our parameter space that we called the attractor.

### 3.3 Result

We therefore wished to define an algorithm that could rule-out, or confirm, RI as a contributing mechanism. To that

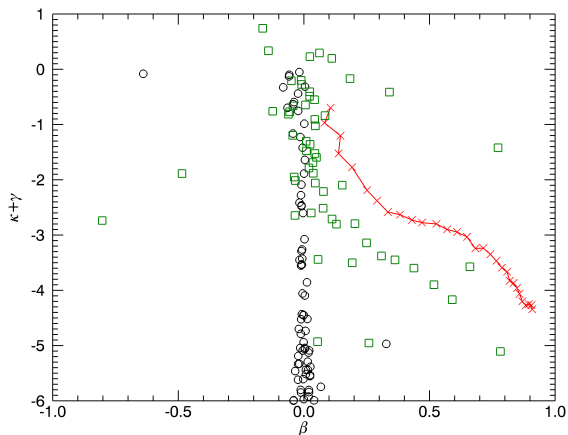


**Figure 2.** Plot showing the system’s progress towards the attractor using the energy-adding kick. Each point represents a mass bin of 5,000 particles and the red line is the position of the attractor. Black circles show bins from the initial conditions whilst green squares are likewise the state *after 5 kicks*.

end we designed the simple kick outlined above, based on the same algorithm of random numbers as in B12. The key difference is that the kick is now asymmetrical, only ever adding energy to a bin, never removing it, and we do not enforce any kind of energy conservation after the kick. The idea is that the system will expand as a result of the added energy and is thus not placing more particles on radial, inwards orbits, preventing a collapsing state, and thus not triggering either RI or ROI.

If the system did not evolve towards the attractor or evolved in a completely different manner now that any kind of infall was being prevented then that would suggest that RI was an important, necessary factor.

Figure 2 shows a plot of the attractor for this kick. The open shapes are bins of 5,000 particles each and the red line is data from Hansen et al. (2010) that marks the position of the attractor in the parameter space. The system shows, despite the unrealistic kick, significant evolution towards the same space as the attractor; from the black circles to the green squares. It is not sitting directly on the attractor but this is, as discussed previously, because of the amount of unbound material causing the simulation to end prematurely. The system was showing regular evolution towards the attractor which slowed in proportion to the amount of unbound material.

We conclude from this that neither RI nor ROI are driving the convergence as repeated expansions still lead to the attractor. This is in agreement with Sparre & Hansen (2012b) where different perturbations were presented, all of which lead to the attractor even in cases where the structures remained perfectly spherical throughout.

## 4 TESTING THE REQUIREMENTS

Having demonstrated that ROI is not the driving force behind the attractor we now consider possible origins discussed in the literature, namely energy exchange and phase mixing

in a dynamic potential. We will show that those two effects are both necessary and sufficient conditions for the emergence of the attractor. Since these effects are always present during mergers this shows the potential importance of the attractor for cosmological collisionless structures (Ludlow et al. 2010).

Energy exchange refers to energy being passed between particles by gravitational interaction. While it may seem that any evolving system must exchange energy to evolve, it is possible to design perturbations that change the system without exchanging energy between particles. For example, one could design a kick which moved the system in phase space by rotating velocity vectors, which would perturb the system but would not cause the particles to exchange energy; they would all still be on stable orbits since their kinetic and potential energies are identical to their previous ones, hence the radial regions indicated by the apocenters of the particles barely change while the pericenters move because of kicks of the angular momentum.

#### 4.1 Energy exchange: the velocity anisotropy axis kick

In order to investigate the importance of energy exchange between collisionless particles, we will now construct a kick which conserves the energy of each particle.

The new kick, which we will refer to as the ‘anisotropy kick’, kicks in velocity isotropy only. It aims to move the system in  $\beta$  by rotating each particle’s velocity vector by a calculated amount. This does not change the total energy in the bin - each particle independently and exactly conserves its kinetic and potential energy - but does, by definition, change the angular momentum. The means by which the velocity rotations are performed is outlined in appendix A. The foundation of the method remains the same as from previous examples; alternating patterns of kick and flow, only now the kick is a function that rotates velocity vectors rather than randomly scaling individual components of velocity.

The resulting system will be slightly Radially Jeans Unstable (RJU), i.e. not satisfying the static spherical Jeans equation, after the kick so the system will still need to re-establish equilibrium. This kick should require the system to find a new equilibrium but does so without a prescribed way that the new equilibrium is reached.

We first take an initial system with a radially anisotropic velocity ellipsoid and force it to become more isotropic. Figure 3 examines the change in the velocity anisotropy of the system as it equilibrates after the kick. We define the ‘change in velocity anisotropy’ simply as  $\frac{\Delta\beta}{\Delta t}$  where  $\Delta t$  is time between outputs of the state of the system *i.e.*  $0.01T_{dyn}$ . The kick is visible as the large, dark blue section at the beginning of the time series. Afterwards, the system relaxes over the course of about a dynamical time. The relaxation is visible in the yellow-green tint across the rest of plot, showing a general trend for the system to drift towards a more radial velocity anisotropy again. See figure 4 for an alternative representation of some of the information displayed in figure 3.

There are two particularly prominent features in figure 3 that require comment. The first is the kick itself, clearly visible as a large, dark area along the left side, and the other is the ‘sawtooth’ pattern of spikes in velocity anisotropy rate

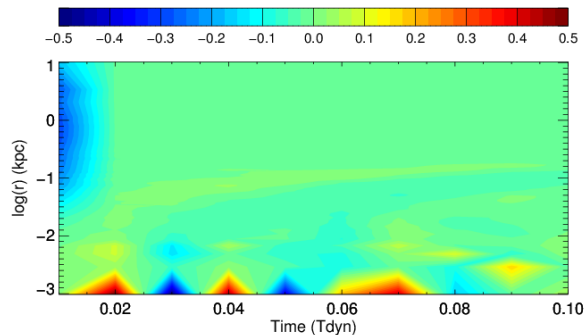


**Figure 3.** Contours showing the changes in velocity anisotropy of an initially radially anisotropic system as it recovers from a moderately isotropising kick. As the system relaxes over time after being kicked, it is measured every 1% of a dynamical time and the velocity anisotropy of each bin is compared to its previous anisotropy. The change in anisotropy at a certain radius from moment to moment is represented by the colour of the contours, where blue colours indicate an ongoing change towards towards tangential anisotropy and red colours indicate likewise for radial anisotropy. Green represents no evolution of anisotropy between outputs.

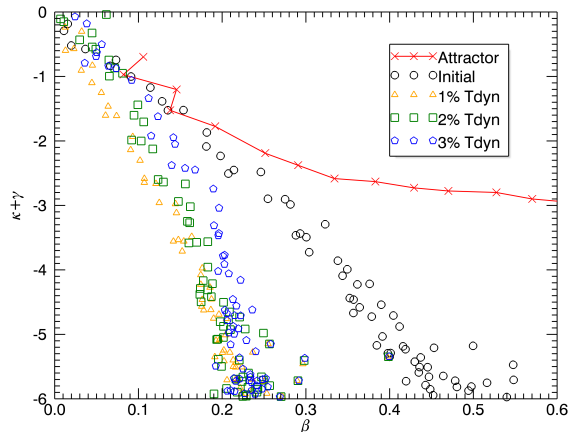


**Figure 4.** A more familiar presentation of some of the datasets represented in figure 3 using the plot axes of the attractor space. Note the gentle drift of the data towards radial anisotropy during the first 3% of a dynamical time after the kick, as summarised in figure 3 by the yellow-green hue of the majority of the contours.

that run along the bottom of the graph. Both of these features overshadow the actual point of interest, the general trend of the plot, and accordingly all future plots will be cropped and re-scaled to present the clearest view of the data. We will now take a moment to justify the removal of these features.

Firstly, removing the kick is regrettable but it is of such greater magnitude than anything else in the plot that retaining it over-saturates the important contours. The only useful information that it contained was the colour (direction) of the kick which will always be indicated.

Secondly, the ‘sawtooth’ pattern that appears at very small radii is caused by an unfortunate combination of two

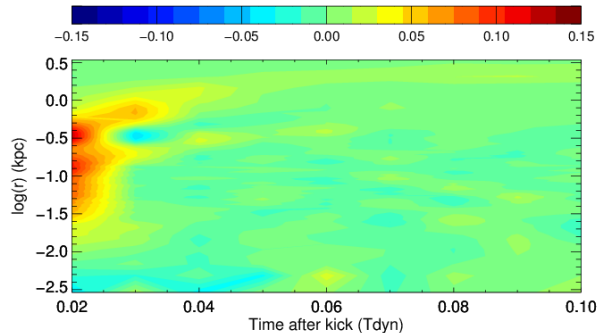


**Figure 5.** Contours showing the changes in velocity anisotropy of an initially radially anisotropic system as it recovers from a kick that set it to be completely isotropic. Notice that the system recovers by settling back towards radial anisotropy like figure 3, only much more strongly. Also note that, in line with the discussion in the body text and in contrast to figure 3, the oversaturated noise and kick features have been removed. Thus, the reddish spot along the left is not the kick, but the resettling of the system after the kick has occurred.

factors: the logarithmic scale artificially overemphasising the relative importance of the inner bins (in terms of how much of the contour area they occupy), and the tendency for the very innermost bins to have an extremely noisy velocity anisotropy as a result of the data analysis. Clipping those few bins cleans the data considerably, removes only a small amount of particles, and does not destroy any useful information.

The amount of settling is a negative feedback effect that is a fraction of the size of the perturbation. For example, if the system is initially strongly radial and the kick is strong enough to make the system isotropic then the settling will act to reverse the kick by drifting towards radial states, as seen in figure 5. This drifting is stronger and more pronounced the larger the initial kick and is never enough to undo the kick.

We will now demonstrate that this negative feedback is not related to the attractor. In figure 6 we take an initially tangentially anisotropic system and perturb it towards isotropy. What we see is the reverse of figure 3 with the settling being more tangential and thus a light blue.

This demonstrates that when a system is perturbed using the anisotropic kick its subsequent relaxation will undo a small fraction of that isotropy change. This means that while this perturbation does destabilise the system and allow it to find new equilibria, it does not lead towards the attractor.

In our final test of this, we took an initially slightly radially anisotropic system and repeatedly perturbed it such that the system gradually moved up to, and then past, the phase-space region of the attractor. The reasoning behind this scheme is that if the system is still affected by the attractor then we would expect it to behave differently when it is passing over it, perhaps changing the magnitude or direction of the settling.

We found that none of the kick-flow cycles in the series showed any evidence of being drawn to the attractor. The velocity anisotropy evolution remained comparatively fea-

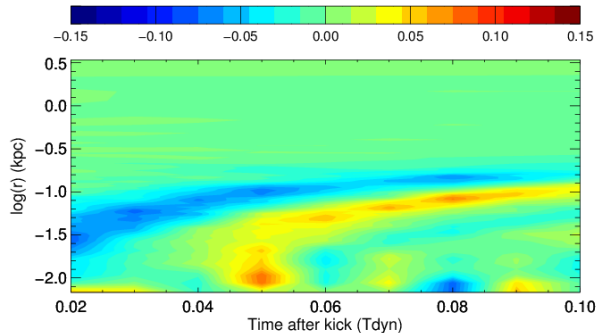


**Figure 6.** Contours showing the changes in velocity anisotropy of an initially tangentially anisotropic system as it recovers from an isotropic kick. The green-blue hue of most of the plot, demonstrating motion towards tangential anisotropy, shows that settling is not directed towards the attractor. The two large stripes across the plot are the equivalent of the dark spot in figure 5 and are the settling of the system against the kick. Here the settling is towards a more tangential anisotropy and occurs as a ripple of anisotropy through the system from the inner regions to the outer. This effect is still minor compared to the kick and overall does still obey the established rule.

tureless throughout and showed no behaviour different from any other system perturbed by the anisotropic kick.

Overall, it appears that this method of perturbing the system does cause the system to undergo some slight evolution in response to the kick, but it seems restricted to a weak, negative feedback effect that bears no relation or correlation to the attractor.

#### 4.2 Phase mixing in a fixed potential: the massless kick

By phase mixing we mean how particles disperse through the phase space of the system, generally reducing the coarse grained phase-space density by filling their orbital tori evenly. This is a kinematic process that causes a dispersion of particles along their orbits which even occurs in static potentials (Binney & Tremaine 2008) and corresponds to the processes that occur during the ‘flow’ periods of our perturbation schemes. In B12 we showed that repeated kicks, without subsequent periods of settling flow, do not lead to the attractor. Here we will further emphasise the importance of the dynamics of the flow by considering relaxation in a fixed potential.

This perturbation involved making the particles massless. We took the same initial plummer spheres as before but then froze the system’s numerical, not analytical, potential and transformed the particles into a population of massless tracer particles. This means the background potential is no longer coupled to the particle distribution and, because the simulation is collisionless, the particles have no way of interacting with each other. After the kick has occurred the particles will not be able to directly influence each others positions in phase space.

If the attractor is driven only by the kick then removing the dynamical potential should have minimal effect on the system’s convergence to the attractor as simply the act of kicking would cause convergence.

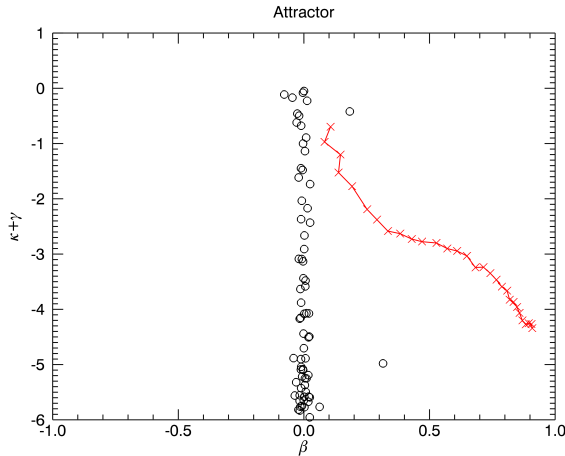


**Figure 7.** A plot showing an initially anisotropic system after an application of the ‘massless kick’. Comparison between the current system and its initial state is made difficult as the system has not evolved at all as a result of the kick. The black circles are bins of the system after one kick and were completely unaffected by the kick. The red line is the attractor.

We show the effects of applying the normal scaling kick of B12 to our massless system in figure 7. The system has not evolved since the kick and has certainly not moved towards the attractor. This shows that the attractor does not arise from the statistics of the kick mechanism alone and does in fact require the subsequent mixing in a dynamical potential. Such mixing in a dynamical potential is fortunately always present during realistic cosmological structure formation.

## 5 SUMMARY

We have addressed the fundamental physical mechanism responsible for the attractor. We find that the radial orbit instability is not the underlying reason for the robustness of the attractor.

Instead, we find that both energy exchange and phase mixing in a dynamical potential are necessary conditions for the appearance of the attractor. Since earlier studies have indicated that those two are sufficient conditions (Sparre & Hansen 2012a,b), we believe we have established the physics underlying the attractor. Since both effects are present during structure formation, in particular through violent relaxation of mergers, this shows that the attractor is relevant for the fully equilibrated part of cosmological structures.

## 6 ACKNOWLEDGEMENTS

The authors gratefully acknowledge the invaluable help and input of Xufen Wu of the University of Bonn. The Dark Cosmology Centre is funded by the Danish National Research Foundation. This research was funded in part by the Science and Technology Facilities Council.

## REFERENCES

- An J. H., Evans N. W., 2006, *The Astrophysical Journal*, 642, 752
- Antonov V. A., 1973, in Omarov T. B., ed., *Dynamics of Galaxies and Star Clusters On the instability of stationary spherical models with merely radial motions.* pp 139–143
- Barber J. A., Zhao H., Wu X., Hansen S. H., 2012, *Monthly Notices of the Royal Astronomical Society*, 424, 1737
- Barnes E., Williams L., Babul A., Dalcanton J., 2005, *The Astrophysical Journal*, 634, 775
- Bellovary J., Dalcanton J., Babul A., Quinn T., Maas R., Austin C., Williams L., Barnes E., 2008, *The Astrophysical Journal*, 685, 739
- Binney J., Tremaine S., 2008, *Galactic Dynamics*, second edn. Princeton Series in Astrophysics, Princeton University Press
- Ciotti L., Londrillo P., Nipoti C., 2006, *The Astrophysical Journal*, 640, 741
- Ciotti L., Morganti L., 2010, *Monthly Notices of the Royal Astronomical Society*, 408, 1070
- Dubinski J., Carlberg R. G., 1991, *The Astrophysical Journal*, 378, 496
- Gerhard O., 1991, *Monthly Notices of the Royal Astronomical Society*, 250, 812
- Hansen S. H., 2004, *Monthly Notices of the Royal Astronomical Society*, 352, L41
- Hansen S. H., Juncher D., Sparre M., 2010, *The Astrophysical Journal*, 718, L68
- Hansen S. H., Moore B., 2006, *New Astronomy*, 11, 333
- Hansen S. H., Moore B., Zemp M., Stadel J., 2006, *Journal of Cosmology and Astroparticle Physics*, p. 14
- Hernquist L., 1990, *The Astrophysical Journal*
- Hernquist L., Ostriker J. P., 1992, 386, 375
- Hernquist L., Spergel D. N., 1992, *The Astrophysical Journal Letters*, 399, L117
- Huss A., Jain B., Steinmetz M., 1999, *The Astrophysical Journal*, 517, 64
- Lapi A., Cavaliere A., 2011, *The Astrophysical Journal*, 743, 127
- Ludlow A., Navarro J., Springel V., Vogelsberger M., Wang J., White S. D. M., Jenkins A., Frenk C. S., 2010, *Monthly Notices of the Royal Astronomical Society*, 406, 137
- Macmillan J.D. and Widrow L., Henriksen R., 2006, *The Astrophysical Journal*, 653, 43
- Navarro J. F., Frenk C. S., White S. D. M., 1996, p. 255
- Sparre M., Hansen S. H., 2012a, *Journal of Cosmology and Astroparticle Physics*, 7, 42
- Sparre M., Hansen S. H., 2012b, *Journal of Cosmology and Astroparticle Physics*, 10, 49
- Syer D., White S. D. M., 1998, *Monthly Notices of the Royal Astronomical Society*, 293, 337
- Taylor J. E., Navarro J. F., 2001, *The Astrophysical Journal*, 563, 483
- Zhao H., 1996, *Monthly Notices of the Royal Astronomical Society*, 278, 488

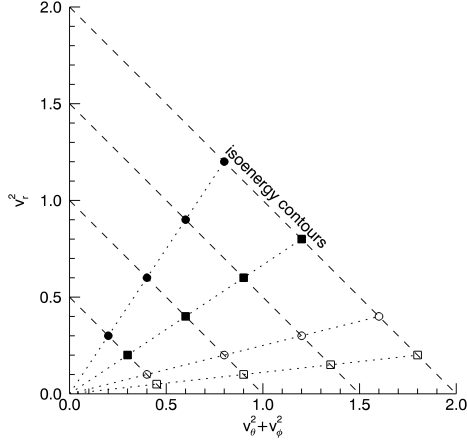


**Figure A1.** A visual representation of how the perturbation changes anisotropy. Particles are moved along isoenergy contours from the open symbols to the closed symbols. This plot shows a kick of  $\alpha = 6$  applied to two groups of particles, one with most of their energy in the tangential velocity components (squares) and the other with a more even distribution (circles). The distance moved along the isoenergy contours depends on the particle's initial position along them.

## APPENDIX A: CONSTRUCTION OF THE ISOTROPISING KICK

The nomenclature used in this section is as follows: A bin in our system has a population of  $n$  particles that give the bin an anisotropy of  $\beta$  based on their kinetic energy,  $T$ , in the radial,  $T_r$ , and tangential,  $T_t$ , directions;  $T_t$  being made up of  $T_\theta$  and  $T_\phi$ . We are talking about a perturbation, so we speak in terms of an *initial* state,  $\beta_1$ , and a *final* state,  $\beta_2$ . We find it helpful to specifically define  $T_t$  as  $\frac{1}{2}(T_\theta + T_\phi)$  as this simplifies matters.

As such, we begin from:

$$\beta_1 = 1 - \frac{\sum_{i=1}^n T_{t1i}}{\sum_{i=1}^n T_{r1i}} \quad (\text{A1})$$

Our perturbation acts to move the anisotropy from  $\beta_1$  to  $\beta_2$ , the change being expressed as:  $x\beta_1 = \beta_2$ , so we can say:

$$x\beta_1 = 1 - \frac{\sum_{i=1}^n T_{t2i}}{\sum_{i=1}^n T_{r2i}} = 1 - \frac{a(x) \sum_{i=1}^n T_{t1i}}{b(x) \sum_{i=1}^n T_{r1i}} \quad (\text{A2})$$

where  $a$  and  $b$  are just another, more helpful way of assessing the impact of  $x$  on the particle energies. Speaking of the particle energies, we require global energy conservation, so we specify that:

$$2a(x) \sum_{i=1}^n T_{t1i} + b(x) \sum_{i=1}^n T_{r1i} = 2 \sum_{i=1}^n T_{t1i} + \sum_{i=1}^n T_{r1i} = \mathcal{E} \quad (\text{A3})$$

where  $\mathcal{E}$  is the system's overall kinetic energy. We can thus create definitions of  $a$  and  $b$ ,

$$a(x) = \frac{\mathcal{E} - b(x) \sum_{i=1}^n T_{r1i}}{2 \sum_{i=1}^n T_{t1i}}; b(x) = \frac{\mathcal{E} - 2a(x) \sum_{i=1}^n T_{t1i}}{\sum_{i=1}^n T_{r1i}} \quad (\text{A4})$$

and feed them into each other to get solutions that are still linked by energy conservation but can be expressed separably;

$$a(x) = \frac{\mathcal{E}}{\sum_{i=1}^n T_{t1i} \left[ 2 + \frac{1}{1-x\beta_1} \right]}; b(x) = \frac{\mathcal{E}}{\sum_{i=1}^n T_{r1i} [3 - 2x\beta_1]} \quad (\text{A5})$$

This tells us how the bin as a whole must act, but does not tell us how to achieve this by manipulating individual particles. To move on to that stage we must make  $a$  and  $b$  more applicable to each particle.

When we scale the tangential energy,  $\sum_{i=1}^n T_{t1i}$ , by  $a$ , what we are actually doing is multiplying each particle's energy by some number, quite possibly a *different number for each of them*, and we need a way to determine what that number should be. To that end, we create two numbers,  $d$  and  $e$ , and let them take different values for each particle,  $i$ .

For convenience we do not write out the dependence of  $d$  and  $e$  on  $a$  *vis. d(a)\_i*. This is primarily to reduce clutter and because the final result of the process will not need to refer to  $a$ ,  $b$ , or any of the other scale factors introduced in this process.

$$\sum_{i=1}^n T_{t2i} = a(x) \sum_{i=1}^n T_{t1i} = \sum_{i=1}^n d_i T_{t1i} = \frac{\mathcal{E}}{1 + \frac{1}{1-x\beta_1}} \quad (\text{A6})$$

$$\sum_{i=1}^n T_{r2i} = b(x) \sum_{i=1}^n T_{r1i} = \sum_{i=1}^n e_i T_{r1i} = \frac{\mathcal{E}}{2 - x\beta_1} \quad (\text{A7})$$

As well as global energy conservation, we now specify that we would like energy conservation at the particle level as well:

$$2d_i T_{t1i} + e_i T_{r1i} = 2T_{t2i} + T_{r2i} = E_i \quad (\text{A8})$$

At this point it is most convenient to start constructing the problem in terms of a single variable that we must solve for,  $\alpha$ :

$$\frac{T_{t2i}}{T_{r2i}} = \frac{d_i T_{t1i}}{e_i T_{r1i}} = \alpha_i \frac{T_{t1i}}{T_{r1i}} \quad (\text{A9})$$

This allows energy conservation to be rephrased in ways such as:

$$\left[ 2\alpha_i \frac{T_{t1i}}{T_{r1i}} + 1 \right] e_i T_{r1i} = E_i \quad (\text{A10})$$

By manipulating energy conservation in this way, we arrive at the definitions:



$$d_i T_{t1i} = \frac{E_i}{2\alpha_i \frac{T_{t1i}}{T_{r1i}} + 1} \alpha_i \frac{T_{t1i}}{T_{r1i}} \quad (\text{A11})$$

and:

$$e_i T_{r1i} = \frac{E_i}{2\alpha_i \frac{T_{t1i}}{T_{r1i}} + 1} \quad (\text{A12})$$

By taking these results back to equations A6 and A7 and then combining them with our starting point of equation A2, we arrive at our final result:

$$\frac{\sum_{i=1}^n \frac{E_i}{2\alpha_i \frac{T_{t1i}}{T_{r1i}} + 1} \alpha_i \frac{T_{t1i}}{T_{r1i}}}{\sum_{i=1}^n \frac{E_i}{2\alpha_i \frac{T_{t1i}}{T_{r1i}} + 1}} = 1 - x\beta_1 \quad (\text{A13})$$

There are a lot of solutions sets for  $\alpha$  that will yield the result we want and we have no way of choosing between them without stating another condition. The condition we set is that  $\alpha$  has one fixed value for each mass bin, and then we solve the equation iteratively.

This paper has been typeset from a  $\text{T}_\text{E}\text{X}/\text{L}^\text{A}\text{T}_\text{E}\text{X}$  file prepared by the author.